1-20-2006

Simulating the Affects of Glutamatergic Afferents on the Firing Pattern of Midbrain Dopamine Neurons

Richard Spencer Landry Jr.
University of New Orleans

SIMULATING THE AFFECTS OF GLUTAMATERGIC AFFERENTS ON THE FIRING PATTERN OF MIDBRAIN DOPAMINE NEURONS

A Thesis

Submitted to the Graduate Faculty of the
University of New Orleans
in partial fulfillment of the
requirements for the degree of

Master of Science
in
Applied Physics

by

Richard Spencer Landry, Jr.

B.S.E. Tulane University, 2001

December, 2005

ACKNOWLEDGEMENTS

Dr. Carmen Canavier	Department of Psychology University of New Orleans New Orleans, Louisiana
Dr. Alexander Komendantov	Department of Neuroscience Tulane University New Orleans, Louisiana
Dr. Sorinel Oprisan	Department of Psychology University of New Orleans New Orleans, Louisiana
Dr. Ashok Puri	Department of Physics University of New Orleans New Orleans, Louisiana
Dr. John Hegseth	Department of Physics University of New Orleans New Orleans, Louisiana
Dr. Joseph Murphy	Department of Physics University of New Orleans New Orleans, Louisiana

TABLE OF CONTENTS

LIST OF FIGURES

ABSTRACT

A computational model of a midbrain dopamine neuron was extended in this study to include a response to random excitatory afferent input by incorporating the receptor components AMPA and NMDA. In a diagonal band where average glutamatergic and tonic gabaergic input is roughly balanced, both single spike firing and bursting can be observed. Simulated SK channel block strengthens the correlation between pattern and rate and increases the number of spikes fired in bursts by increasing the spikes per burst. A simulated doubling of the AMPA/NMDA ratio leads to a frequency increase that becomes more prominent at high firing rates, and an increase in the percent spikes fired in bursts. Changes in pattern and rate are poorly correlated in the model. Manipulations of the neuron greatly depend on the background level of synaptic inputs, suggesting that interpretation of population data from dopamine neurons requires taking variability into account rather than averages.

INTRODUCTION

DA neurons can be found in the midbrain specifically in the ventral tegmental area (VTA or A10), the substantia nigra pars compacta (SNC or A9), and the retrorubral area (A8). They branch out to the neostriatum, the limbic system, and the cortex (Canavier, 1999). Due to their considerable connectivity, DA neurons are responsible for many brain functions, including the control of movement and motor functions, reward mediated learning, attention, cognitive functionality, and motivation. The destruction of DA neurons through degeneration or cell death results in loss of this functionality and as such has been linked to Parkinson's disease and a variety of mental complications, including schizophrenia, attention deficit disorders, drug addiction, and depression.

DA neurons are responsible for a variety of firing patterns *in vivo* and *in vitro* through the introduction of pharmacological agents. *In vivo* there are two types of firing patterns observed: single spike firing, and burst firing. *In vitro* the burst firing is lost and only single spike firing (the pacemaker-like oscillations) is naturally present (Canavier, 1999). Burst firing can however be induced by the introduction of apamin, a chemical component of bee poison that functions as a calcium dependent potassium channel blocker, or by the introduction of NMDA into the slice preparation. Thus apamin and NDMA are experimentally significant in that they closely resemble the more common activities of DA neurons in a living system. The endogenous firing present in the slice preparation and two types of induced burst firing have been observed *in vitro*. The slow calcium dynamics bring rise to the SOP, and the NMDA induced burst firing relies on mechanisms that are both sodium and voltage dependent. The slow oscillations in the membrane potential are better observed after blocking the action potentials with TTX. By the subsequent application of apamin, the SOP can be converted into a square-wave composed of burst firings

during the peaks of oscillation. Some trials of apamin application resulted in irregular firing instead of burst firing (Canavier 1999 and Komendantov et al. 2003).

Although DA neurons in the SN and VTA fire spontaneous action potentials *in vitro*, afferent inputs to these neurons also produce the same variety of firing modes *in vivo*, ostensibly due to an early depolarization mediated by glutamate followed by a hyperpolarization through the inhibitory effects of GABA (Johnson, 1998). Thus *in vivo*, we are permitted to see both single spike firing, which is characterized by low dopamine release, and burst firing, where the spikes are clustered in groups and two to three times more dopamine is released. The bursting mode of firing is particularly important as it signifies phasic release of dopamine into the postsynaptic cleft, enabling behavioral regulation. The bursting rate due to afferent stimuli has been shown to increase as compared to bursts observed outside of the task context, indicating transient bursting behavior is largely dependent upon occurrence of an event elicited from another neuron. It is also speculated that dopamine neurons may release colocalized peptides during the bursting. Single spike firing is often irregular, but regular single spike firing patterns have been observed in certain experiments involving the freely moving rat (Hyland et al., 2002). DA neurons *in vivo* predominantly fire irregularly, but it should also be noted that the two types of firing patterns present in DA neurons are not necessarily mutually exclusive.

Glutamate is the chief neurotransmitter responsible for fast-responding excitatory signals within the CNS. It is responsible for long term potentiation and plays a critical role in cortical and hippocampal cognitive function, pyramidal and extrapyramidal motor function, cerebellar function, memory, and sensory function. Glutamate is also the precursor for the major inhibitory neurotransmitter GABA. Postsynaptic receptors activated by glutamate are located on the surface of virtually all neurons. Three identified ionotropic receptor subtypes activated by

glutamate are NMDA, alpha-amino-3-hydroxy-5-methyl-4-isoxazolepropionic acid (AMPA), and kainate. The NMDA receptor complex possesses a relatively high calcium permeability which, at the resting neuronal membrane potential (around -70 mV), is blocked by magnesium. When the neuron is depolarized the magnesium block is removed, permitting glutamate to activate the NMDA receptor. AMPA, like NMDA, are receptors that are widely expressed in the CNS and are responsible for most glutamate mediated rapid excitatory neurotransmission. Sustained activation of AMPA receptors by a train of impulses arriving at a pre-synaptic terminal depolarizes the post-synaptic cell, releasing the channel inhibition and thus allowing NMDA receptor activation. Kainate receptor expression is more restricted and appears to play a role in the regulation of neurotransmitter release, but it will not be addressed in the current modeling study.

As the reuptake of glutamate released from axonal terminals to the synaptic cleft is fast and highly efficient, the activation of presynaptic receptors AMPA and NMDA is accordingly rapid. Glutamate binding onto a non-NMDA such as AMPA receptor opens non-selective cation channels more permeable to sodium and potassium than calcium. (Mayer and Westbrook, 1987) Glutamate binding elicits a rapidly activating inward current at membrane potentials negative to 0 mV, and an outward current at potentials positive to 0 mV. Kainate, quisqualate, and AMPA are the specific agonists at these receptors, and 6-cyano-7-nitroquinoxaline-2,3-dione (CNQX) is an antagonist. NMDA-gated currents typically have slower kinetics than AMPA-gated channels. (Bonci and Malenka, 1999).

The model study investigates the response of a DA neuron to external afferent input. Varied concentrations of the neurotransmitter glutamate have been observed as input to a simple kinetic scheme for NMDA and AMPA receptor activation at the postsynaptic terminals of a DA

neuron. Our study evaluates conditions which would correspond to the intact mammal to better understand the patterned output of the DA neuron.

BACKGROUND

The nerve cell, or neuron, is the basic anatomical unit of the nervous system. Every neuron is composed of a cell body, or soma, and branching tubular processes filled with cytoplasm that serve to propagate nerve impulses. Dendrites and axons, the two types of tubular nerve fibers, extend from the cell body and conduct electrical signals. The dendrites are short and branched and function mainly as receptive terminals for the nerve impulses. Axons are slender cylindrical processes responsible for transmitting the nerve impulses to other nearby neurons via synaptic junctions.[1] Figure 1 is a generalized picture of a neuron.

Figure 1: Neuron Anatomy

DA neurons are located in the midbrain in three locations and branch out to the neostriatum, the limbic system, and the cortex.[2] Due to this considerable connectivity, DA

[1] Hole, John W. Jr., and Karen A. Koos. Human Anatomy 2d edition. Dubuque: Wm. C. Brown Publishers, 1994. pp. 266-274.

[2] Canavier, C. C. "Sodium Dynamics Underlying Burst Firing and Putative Mechanisms for the Regulation of the Firing Pattern in Midbrain Dopamine Neurons: A Computational Approach." Journal of Computational Neuroscience. 6: 49, 1999.

neurons are responsible for many brain functions, including the control of movement and motor functions, reward-mediated learning, attention, cognitive functionality, and drug addiction. The loss of DA neurons through degeneration or cell death results in loss of this functionality and as such has been linked to Parkinson's disease and a variety of mental complications, including schizophrenia, attention deficit disorders, and depression.[3]

Nerve tissue is excitable, meaning that it can generate electrochemical impulses and conduct these signals along the surface of the membrane. The transmembrane voltage of a nerve cell is the potential of the inner surface relative to that of the outer surface of the cell membrane. The four general types of transmembrane potentials associated with neurons are the resting potential, pacemaker potentials, synaptic potentials, and potentials resulting from synaptic potentials. The resting potential is the unexcited state of the neuron. Pacemaker potentials are associated with intrinsic electrical oscillation activities of the cell without any external excitation. Synaptic potentials in the cell are due to excitations from external sources. Consequences of synaptic potentials are further subdivided into electrochemical responses dependent upon the magnitude of the input. Nonpropagating, or electrotonic, responses to synaptic potentials result when the stimulus magnitude does not exceed the threshold of the cell membrane. Action potentials arise from excitatory stimuli above threshold. The response is often referred to as an all-or-nothing phenomenon, because once a nerve cell receives a stimulus greater than the membrane threshold, the action potential generated propagates unattenuated along the nerve fiber. Otherwise, if threshold is not achieved, the action potential does not occur.

---

[3] Amini, B., J. W. Clark, Jr., and C. C. Canavier. "Calcium Dynamics Underlying Pacemaker-Like and Burst Firing Oscillations in Midbrain DA Neurons: A Computational Study." Journal of Neurophysiology. 82: 2249, 1999.

Nerve stimulation can either be excitatory, associated with depolarization of the cell membrane, or inhibitory, associated with hyperpolarizing the membrane.[4]

The electrical operation of the nervous system as well as any other excitable tissue is dependent upon electrochemical gradients and the distribution of extracellulari and intracellular ion concentrations. The selective permeability of the nerve cell membrane allows for active transport of certain ions against the concentration gradient. Figure 2 depicts a typical excitable cell membrane and the concentrations of ions in the intracellular and extracellular fluid.[5]

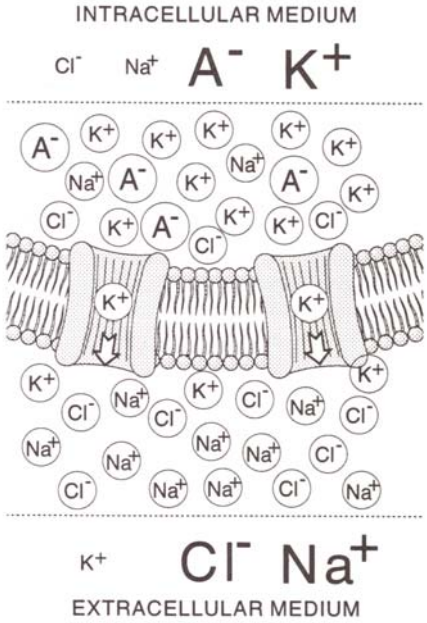

Figure 2: Concentrations of Significant Ions Surrounding Excitable Cells[6]

The metabolically mediated sodium, potassium, and calcium pumps play a crucial role in maintaining the rest polarization of a nerve cell membrane at a negative potential. The typical

[4] Malmivuo, Jaakko, and Robert Plonsey. Bioelectromagnetism. New York: Oxford University Press, 1995. pp. 33-39.
[5] Mead, Carver. Analog VLSI and Neural Systems. New York: Addison-Wesley Publishing Company, Inc., 1989. pp. 43-48.
[6] Malmivuo and Plonsey, p. 47.

nerve cell actively expels sodium ions from the intracellular fluid and accepts potassium ions from the extracellular fluid. When a nerve cell becomes selectively permeable to one or more ions, these ions will diffuse down the concentration gradient, thus changing the net charge of the cytoplasm with respect to the extracellular fluid. At a certain rest potential, the diffusive force of the ions outward will exactly balance with the opposing electric force inward. This balance is described by the Nernst equation, and a general Nernst potential for the kth ion's equilibrium is described below in Equation 0.1:

$$V_k = -\frac{RT}{z_k F} \ln \frac{c_{i,k}}{c_{o,k}} \tag{0.1}$$

V_k = equilibrium voltage for the kth ion [V]

R = gas constant $\left[8.314 \frac{J}{\text{mol} \cdot \text{K}} \right]$

T = absolute temperature $[\text{K}]$

F = Faraday's constant $\left[9.649 \cdot 10^4 \frac{\text{C}}{mol} \right]$

z_k = valence of the kth ion

$c_{i,k}$ = intracellular concentration of the kth ion

$c_{o,k}$ = extracellular concentration of the kth ion

The Nernst equation is suitable for membranes that are permeable to only one type of ion, and thus an extension of these biophysical principles is needed to describe a membrane permeable to several different ions. Utilizing the independence principle that the flux of each ion is independent of the others and the assumption that the membrane has a constant electric field and is uniform, planar, and infinite in its lateral extent, an electro-diffusion model was constructed called the Goldman-Hodgkin-Katz equation. The electric current density of the kth type of ion crossing the membrane is provided for in Equation 0.2:

$$J_k = -\frac{P_k V_m z_k^2 F^2}{RT} \cdot \frac{c_{i,k} - c_{o,k}^{-\frac{V_m z_k F}{RT}}}{1 - e^{-\frac{V_m z_k F}{RT}}} \qquad (0.2)$$

J_k = electric current density of kth ion $\left[\frac{\text{A}}{\text{cm}}\right]$

P_k = permeability of membrane to kth ion $\left[\frac{\text{cm}}{\text{s}}\right]$

V_m = transmembrane potential $[\text{V}]$

Another significant factor in maintaining ionic concentrations on either side of the cellular membrane is the sodium-potassium (Na-K) pump. This is an active transport mechanism responsible for the long-term ionic composition of the space inside and outside of the cell membrane. Recent evidence indicates that the Na-K pump is electrogenic in that two moles of potassium are pumped into the intracellular space for every three moles of sodium pumped out.

A patch of nerve membrane can be described as a nonlinear circuit, where the cell membrane is responsible for the capacitance and selective ion channels responsible for the currents, as shown in Figure 3:

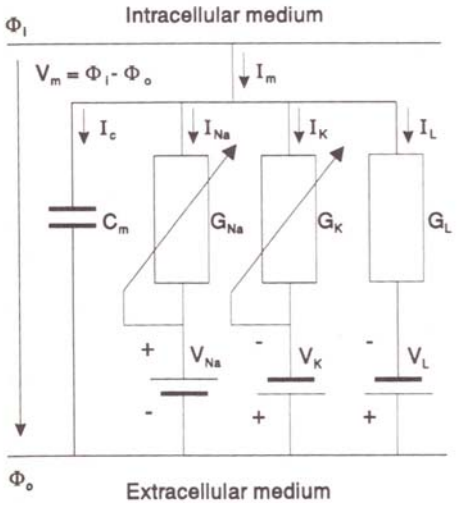

Figure 3: Example of Extracellular Medium

The resistance of the circuit is the part that behaves as nonlinear, and the channels that selectively open for particular ions are voltage dependent.[7] DA neurons are responsible for a variety of firing patterns *in vivo* and *in vitro* through the introduction of pharmacological agents. Midbrain dopamine neurons have a very high depolarizing threshold (-33 ± 15mV).[8] *In vivo*, dopamine neurons exhibit both single spike firing, which is characterized by low dopamine release, and burst firing, where the spikes are clustered in groups and two to three times as much dopamine is released. It is also speculated that dopamine neurons may release colocalized peptides during the bursting. DA neurons *in vivo* predominantly fire irregularly. *In vitro*, the burst firing is lost and only single spike firing, or the pacemaker-like oscillations, is naturally present.[9] Burst firing can however, be induced by the introduction of apamin, a chemical component of bee poison that functions as a calcium dependent potassium channel blocker, or by the introduction of NMDA into the slice preparation. Thus apamin and NDMA are experimentally significant in that they closely resemble the more common activities of DA neurons in a living system. The endogenous firing present in the slice preparation and two types of induced burst firing have been observed *in vitro*. The slow calcium dynamics bring rise to the SOP, and the NMDA induced burst firing relies on mechanisms that are sodium dependent. The slow oscillations in the membrane potential are better observed after blocking the action potentials with TTX. By the subsequent application of apamin, the SOP can be converted into a square-wave composed of burst firings during the peaks of oscillation. Some trials of apamin application resulted in irregular firing instead of burst firing without afferent input.

This project models the pacemaker-like firing and regular burst firing patterns of DA neurons *in vitro* and *in vivo*. The intent is to mimic the behavior of DA neurons under a wide

[7] Mead, p. 48-55.
[8] Clark and Canavier, p. 2249.
[9] Canavier, p. 49-50.

range of experimental conditions. Understanding the mechanisms of calcium and sodium dependent firing patterns observed in vitro is dependent upon knowledge of the responses of the neurons to certain pharmacological agents. In experiment, introduction of TTX to the slice preparation of DA neurons reveals the underlying oscillations in membrane potential, while application of the potassium channel blocker tetraethyl ammonium (TEA) further enhances this intrinsic behavior.

MATERIALS AND METHODS

We used a modified version of the DA neuron from Komendantov and Canavier (2002), where adjustments were made to better fit data from electrophysiological observations and account for afferent inputs. The DA neuron in this computational study was modeled topologically as a cylindrical soma with four slender cylindrical branching dendrites distributed with equal spacing and projecting radially from the soma. The four dendrites were further subdivided into a proximal and distal dendritic compartment, shown in Figure 4:

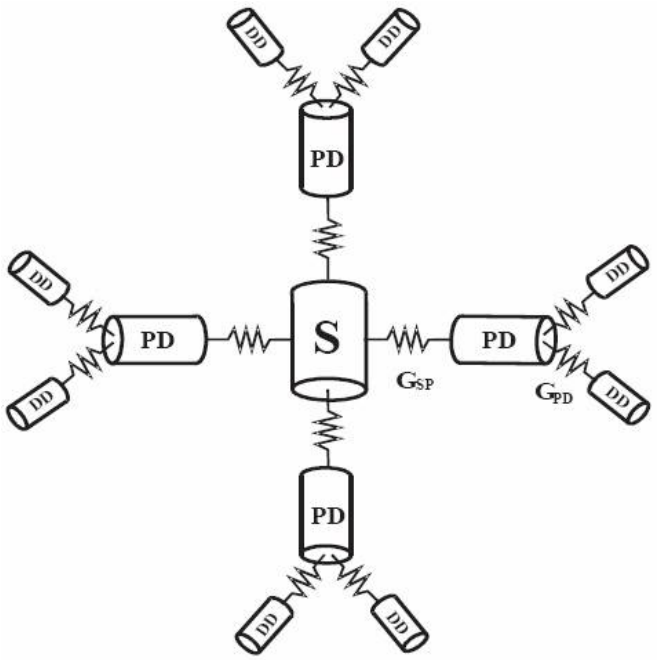

Figure 4: Dopamine Neuron Topology

The soma was modeled as a cylinder 15 μm in diameter and 15 μm in length. The four radially projecting dendrites were modeled as cylinders 500 μm in length with a single change in diameter from 2 μm on the 30% constituting the proximal portion to 1 μm for the remaining

distal 70%. The entire model was constructed using intrinsic quantities. The model assumes a canonical branching structure with four primary dendrites, each having two secondary distal branches. Invoking symmetry, only three electrotonically coupled compartments were integrated - one for the soma (subscript S), one primary, or proximal (subscript P), dendrite and one secondary, or distal (subscript D), dendrite. The distal dendritic portion of the neuron is omitted due to redundancy of the two dendritic sections.

The DA neuron, as it is adapted from a model describing much of the activity under certain conditions *in vitro*, provides an explanation as to how slow oscillations in membrane potential can arise from bath application of NMDA or apamin. It further incorporates the active spiking behavior and burst firing associated with these phenomena. This project models the pacemaker-like firing and regular burst firing patterns of DA neurons both *in vitro* and *in vivo*. The intent is to mimic the behavior of DA neurons under a wide range of live experimental conditions and slice preparations. Understanding the mechanisms of calcium and sodium dependent firing patterns observed *in vitro* is dependent upon knowledge of the responses of the neurons to certain pharmacological agents.

Three systems of differential equations were used to approximate the behavior of the DA neuron, including the axial diffusion of sodium and the electrotonic propagation of current along the cell membrane. The calcium in this model is assumed at steady state in the dendrites, and longitudinal diffusion equations are thus not included for this ion. For ease and speed of the computational simulation, the DA neuron was modeled compartmentally rather than continuously, and due to the symmetry of the dendritic portion the equations were simulated for only one projecting dendrite. The conductances connecting the compartments were estimated using the geometry and biophysical properties of the model (Canavier, 1999).

The salient features of the model are that the dendrites have sodium dynamics including sodium entry via NMDA (I_{NMDA}) and AMPA (I_{AMPA}) receptor channels, a voltage dependent fast sodium channel (I_{Na}), and removal via a sodium potassium pump (I_{NaP}). These sodium dynamics are capable of producing burst firing, and both soma and dendrite possess the currents underlying action potential generation including the fast sodium current (I_{Na}), the delayed rectifier ($I_{K,DR}$), and the transient outward current, ($I_{K,A}$). There are calcium dynamics in the soma including calcium entry via several voltage dependent calcium currents ($I_{Ca,T}$, $I_{Ca,N}$, and $I_{Ca,L}$) and removal via a calcium pump (I_{CaP}). Voltage dependent calcium entry activates small conductance SK potassium channels (I_{SK}), and a tonic level of activation of $GABA_A$ receptor channels ($I_{GABA,A}$) on the soma is used to simulate the input resistance of dopamine neurons *in vivo*. The activation of AMPA and NMDA receptors have temporal dynamics that are calibrated according to published experimental data.

The cell membrane of the DA neuron behaves as a capacitor, and this model provides the DA electric equivalent circuit representation with equivalent capacitances for each of the three compartments (1 $\mu F/cm^2$) shown in Figure 5:

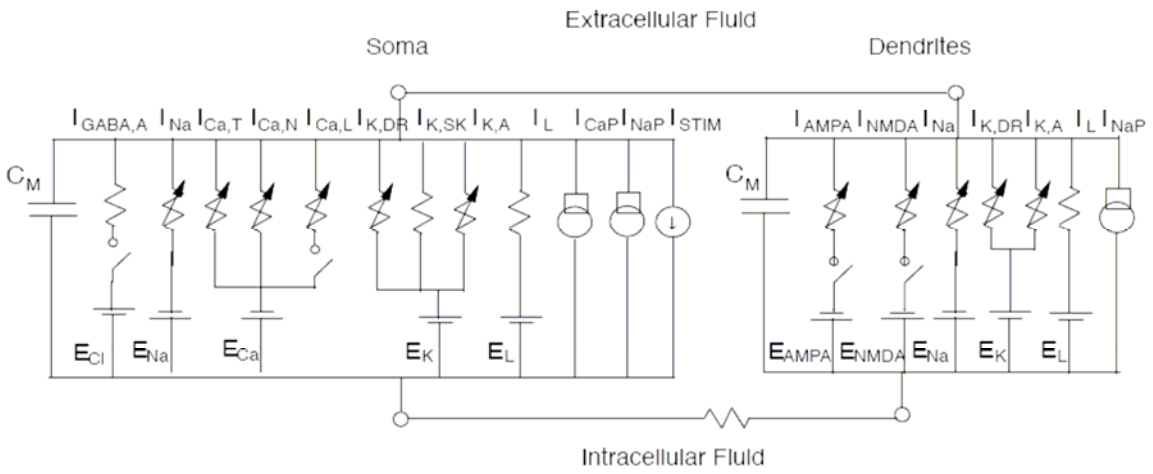

Figure 5: Equivalent Circuit of Dopamine Neuron

The parallel conductance model of the neuron is a Hodgkin-Huxley equivalent circuit described by resistive ion-selective channels, ionic currents, and ion pumps.

The state equations governing the transmembrane potential in each compartment are shown below in Equation 1.1, noting that subscripts for repeated currents in separate compartments are suppressed.

$$
\begin{aligned}
c_m \frac{dV_s}{dt} &= -\left(i_{Ca,T} + i_{Ca,N} + i_{Ca,L} + i_{CaP} + i_{SK} + i_{GABA,A} + i_L + i_K + i_{Na} + i_{NaP} - i_{STIM} - i_{Clamp} + 4i_{sp}\right) \\
c_m \frac{dV_p}{dt} &= -\left(i_L + i_K + i_{Na} + i_{NaP} + i_{GABA,A} + i_{NMDA} + i_{AMPA} + i_{ps} + 2i_{pd}\right) \\
c_m \frac{dV_d}{dt} &= -\left(i_L + i_K + i_{Na} + i_{NaP} + i_{GABA,A} + i_{NMDA} + i_{AMPA} + i_{dp}\right)
\end{aligned}
\tag{1.1}
$$

The fluid compartment model is composed of three types of intracellular compartments containing a constant concentration of Ca^{2+} and K^+, where Na^+ is modeled using the diffusion equation, seen in Equation 1.2. The compartments - somatic, proximal dendritic, and distal dendritic - are modeled similarly except the dendritic section is assumed permeable to AMPA

and sodium related NMDA currents. The extracellular space is assumed very large, so that ionic concentrations of Ca^{2+}, Na^{+}, and K^{+} are constant:

$$\begin{aligned}
\frac{d[Na]_s}{dt} &= -4f_s \frac{i_{Na} + i_{L,Na} + 3i_{NaP} + 4i_{diff,sp}}{d_s F} \\
\frac{d[Na]_p}{dt} &= -4f_p \frac{i_{Na} + i_{L,Na} + 3i_{NaP} + i_{NMDA,Na} + i_{AMPA,Na} + i_{diff,ps} + 2i_{diff,pd}}{d_p F} \\
\frac{d[Na]_d}{dt} &= -4f_d \frac{i_{Na} + i_{L,Na} + 3i_{NaP} + i_{NMDA,Na} + i_{AMPA,Na} + i_{diff,dp}}{d_d F}
\end{aligned} \tag{1.2}$$

Here f_i indicates the reciprocal of the effective volume factor. This modulates the volume possible for sodium accumulation, and takes into consideration the effective volume reduction from cell organelles. The diameters of the cylindrical sections are denoted by d_i.

In a reduced model for the DA neuron where only three compartments are modeled spatially, the approximation for longitudinal current flow is modeled linearly as follows in Equation 1.3:

$$\begin{aligned}
\frac{d}{4R_a}\frac{\partial^2 V}{\partial x^2} &\approx \frac{1}{\pi d_i L_i R_{ij}}\left(V_i - V_j\right) \\
R_{ij} &= \frac{2R_a}{\pi}\left(\frac{L_i d_j^2 + L_j d_i^2}{d_i^2 d_j^2}\right)
\end{aligned} \tag{1.3}$$

Henceforth we have dicretized the compartments for ease of computational simulation, as previous studies (Canavier 1999) have shown the reduced model retains all aspects of the dynamics.

Apamin induced oscillations were modeled approximately by the inclusion of a calcium current and a calcium activated potassium current. The calcium current was modeled as in (Amini et. al. 1999), and the calcium activated potassium current was modeled with the

assumption that the associated channels were located in close proximity to the calcium stores in the cell soma. The equations for the apamin related channels are described in the model by modifying only the preexisting SK type calcium-activated potassium channel used in Komendantov et al. (2003), with a minor adjustment to SK conductance (800 μS/cm^2 instead of 900 μS/cm^2) in order to reflect data depicted in Figure 2B in Komendantov et al. (2003). By analyzing the spike train data (Ping and Shepard, 1996), it has been shown experimentally that apamin has an affect on NMDA-induced burst firing associated with sodium dynamics, which could link the calcium and sodium dynamics in the DA neuron.

The Hodgkin Huxley-type gating variables related to those currents that describe the opening and closing of selective ion channels are solutions to a first order differential equation of the form of Equation 1.4:

$$\frac{dz(V,t)}{dt} = \frac{\bar{z}(V) - z(V,t)}{\tau_z(V)}, \tag{1.4}$$

where $\bar{z}(V)$ is the steady state value of the gating variable and $\tau_z(V)$ is the time constant of the channel mechanism. The steady-state gating variables have a Boltzman-type relationship, and the time constants $\tau_z(V)$ have a Gaussian relationship.

The Nernst equation is suitable for membranes that are permeable to only one type of ion, and thus an extension of these biophysical principles is needed to describe a membrane permeable to several different ions, such as currents responsible for the ionotropic properties of NMDA. Utilizing the independence principle that the flux of each ion is independent of the others and the assumption that the membrane has a constant electric field that is uniform, planar, and infinite in its lateral extent, an electro-diffusion model was constructed called the Goldman-

Hodgkin-Katz equation. The electric current density of the k[th] type of ion crossing the membrane is provided for in Equation 1.5:

$$J_k = -\frac{P_k V_m z_k^2 F^2}{RT} \cdot \frac{c_{i,k} - c_{o,k} e^{-\frac{V_m z_k F}{RT}}}{1 - e^{-\frac{V_m z_k F}{RT}}} \tag{1.5}$$

Here J_k is the electric current density of the k[th] ion, and P_k is the affective permeability of the cell membrane to the k[th] ion.

Bath application of NMDA is modeled in the DA neuron as a series of NMDA induced currents based on the permeability of the membrane to certain ions in the intracellular and extracellular medium. The equations (1.6) for the NMDA and AMPA induced currents are shown below:

$$\begin{aligned}
i_{NMDA,Na} &= P_{NMDA} O_{NMDA} p_\infty \frac{VF^2}{RT} \frac{\lambda[Na]_i - \lambda[Na]_o e^{-\frac{VF}{RT}}}{1 - e^{-\frac{VF}{RT}}} \\
i_{NMDA,K} &= P_{NMDA} O_{NMDA} p_\infty \frac{VF^2}{RT} \frac{\lambda[K]_i - \lambda[K]_o e^{-\frac{VF}{RT}}}{1 - e^{-\frac{VF}{RT}}} \\
i_{NMDA,Ca} &= 10.6 P_{NMDA} O_{NMDA} p_\infty \frac{4VF^2}{RT} \frac{\lambda_{Ca}[Ca]_i - \lambda_{Ca}[Ca]_o e^{-\frac{2VF}{RT}}}{1 - e^{-\frac{2VF}{RT}}} \\
p_\infty &= 0.05 + \frac{0.95}{1 + \frac{[Mg]_o}{K_{m,Mg}} e^{-\frac{V}{q}}} \\
i_{AMPA,Na} &= O_{AMPA} g_{AMPA} \left(V - \frac{RT}{F} \ln\left(\frac{[Na]_o}{[Na]_i} \right) \right) \\
i_{AMPA,K} &= O_{AMPA} g_{AMPA} \frac{RT}{FE_K} \ln\left(\frac{[Na]_i}{[Na]_o} \right) (V - E_K) \\
i_{NMDA} &= i_{NMDA,Na} + i_{NMDA,K} + i_{NMDA,Ca} \\
i_{AMPA} &= i_{AMPA,Na} + i_{AMPA,K}
\end{aligned} \tag{1.6}$$

The open channel gating mechanisms for the NMDA and AMPA receptors are governed by the following simplified kinetic diagrams below in Equation 1.7:

$$\begin{aligned} R_{AMPA} + [Glu] &\underset{k_{off,AMPA}}{\overset{k_{on,AMPA}}{\rightleftharpoons}} O_{AMPA} \\ R_{NMDA} + [Glu] &\underset{k_{off,NMDA}}{\overset{k_{on,NMDA}}{\rightleftharpoons}} O_{NMDA} \end{aligned} \tag{1.7}$$

Here R_{AMPA} and R_{NMDA} stand for the unbound receptors for AMPA and NMDA, and O_{AMPA}, O_{NMDA} are the open states for the AMPA and NMDA receptors, respectively. The differential equations describing the dynamic behavior of the channels are documented below in Equation 1.8:

$$\begin{aligned} \frac{dO_{AMPA}}{dt} &= k_{on,AMPA}[Glu](1 - O_{AMPA}) - k_{off,AMPA}O_{AMPA} \\ \frac{dO_{NMDA}}{dt} &= k_{on,NMDA}[Glu](1 - O_{NMDA}) - k_{off,NMDA}O_{NMDA} \end{aligned} \tag{1.8}$$

The open channel variables act as gates for the AMPA and NMDA current contributions to the model. Assuming steady state values for the gates results in the following equations (1.9):

$$\begin{aligned} O_{AMPA} &= \frac{1}{1 + \frac{k_{off,AMPA}}{k_{on,AMPA}[Glu]}} \\ O_{NMDA} &= \frac{1}{1 + \frac{k_{off,NMDA}}{k_{on,NMDA}[Glu]}} \end{aligned} \tag{1.9}$$

We assume that both the NMDA and AMPA components of glutamate receptor activation obey a simple kinetic scheme shown below in Equation 1.10:

$$R_{off} + [Glu] \underset{\beta}{\overset{\alpha}{\rightleftharpoons}} R_{on} \tag{1.10}$$

If the transmitter glutamate is transported as a pulse to activate receptors, there will be two corresponding functions (Equation 1.11) which govern the behavior of the receptor output, based on the onset and the duration of the pulse of transmitter:

$$\begin{aligned} r_{on}^{n}(t) &= r_{\infty}\left(1-e^{-\tau\left(t-t_{n}\right)}\right) \\ r_{off}^{n}(t) &= r_{\infty}\left(1-e^{-\tau d}\right)e^{-\beta\left(t-\left(t_{n}+d\right)\right)} \end{aligned} \tag{1.11}$$

Here we have made the assumption that the receptor was inactive before the onset of transmitter. The equations are summed together when multiple receptors are activated, and the number of r_{off} and r_{on} functions summed will depend on the point measured in time. Experimental results indicate convergence of the output equations resultant from receptor activations in both the AMPA and NMDA components when multiple events are summed together. This leads to the hypothesis that there is an obtainable analytic form of the total receptor activity. In both the NMDA and AMPA components, the expression for total receptor activity at a time t is given by the following (Equation 1.12):

$$R_{Total}(t) = \sum_{n=0}^{N-1} r_{off}^{n}(t) + \sum_{n=N}^{M} r_{on}^{n}(t) \tag{1.12}$$

Here N and M are the total number of activated receptors in the on and off states, respectively, at time t. Since t_n stands for the point in time signifying the n-th spike in a Poisson-processed spike train, we can assume that on average, $t_n \approx n\langle IEI\rangle$. Furthermore, if we assume the mean interevent interval is greater than the duration of the transmitter pulse, we will have at most only one receptor activated in the on state. In light of this simplification we have (Equation 1.13):

$$\begin{aligned} &\sum_{n=N}^{MAX} r_{on}^{n}(t) \approx r_{\infty}\left(1-e^{-\tau\left(t-N\langle IEI\rangle\right)}\right) \\ &\sum_{n=0}^{N-1} r_{off}^{n}(t) \approx r_{\infty}\left(1-e^{-\tau d}\right)e^{-\beta(t-d)}\sum_{n=0}^{N-1}\left(e^{\beta\langle IEI\rangle}\right)^{n} = r_{\infty}\left(1-e^{-\tau d}\right)e^{-\beta(t-d)}\left(\frac{1-e^{\beta\langle IEI\rangle N}}{1-e^{\beta\langle IEI\rangle}}\right) \end{aligned} \tag{1.13}$$

The total time transpired can be expressed using the total number of activated receptors and the mean interevent interval as $t_{Total} = N\langle IEI\rangle + t_f$, where t_f is some fraction of the mean interevent interval. Consequently, we can calculate the total analytic expression (Equation 1.14):

$$R_{Total}(t) \approx r_\infty \left(\left(1 - e^{-\tau d}\right) e^{-\beta\left(\langle IEI\rangle N + t_f - d\right)} \left(\frac{1 - e^{\beta\langle IEI\rangle N}}{1 - e^{\beta\langle IEI\rangle}} \right) + \left(1 - e^{-\tau t_f}\right) \right) \tag{1.14}$$

As time progresses, we have the following range (Equation 1.15) due to attenuation of exponentials for large N:

$$\begin{aligned} R_{Total}^{MAX}(t) &= r_\infty \left(1 - e^{-\tau d}\right) \left(\frac{e^{\beta\langle IEI\rangle}}{e^{\beta\langle IEI\rangle} - 1} \right) \\ R_{Total}^{MIN}(t) &= r_\infty \left(1 - e^{-\tau d}\right) \left(\frac{e^{\beta d}}{e^{\beta\langle IEI\rangle} - 1} \right) \end{aligned} \tag{1.15}$$

This scheme provides weak bounds for the behavior of the activated receptors. The actual summation depends on a random pulse train with a fixed mean interevent time, and as such the total activity will deviate from the bounds described above. The behavior suggested by the analytical expressions would correspond to a perfectly coherent set of inputs to the neuron.

The calibration of temporal patterning of the currents evoked by glutamate was performed using experimental data from DA neurons:

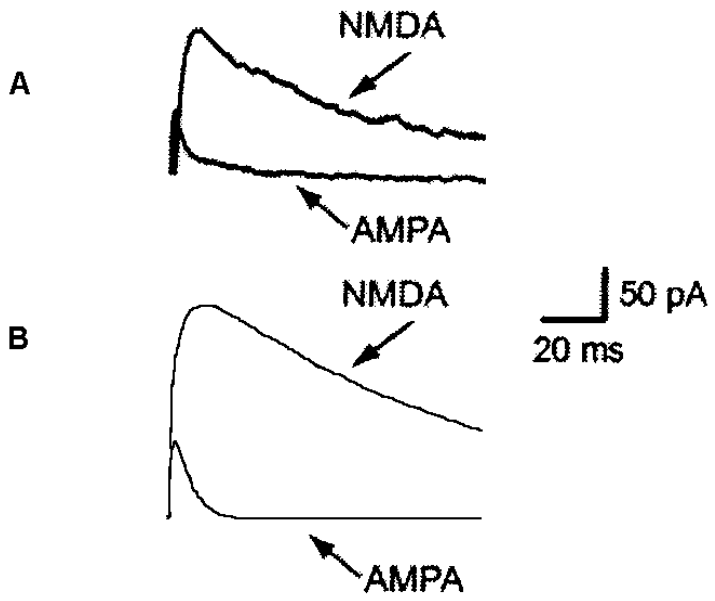

Figure 6: Calibration to Experimental Data

Figure 6A is adapted from Figure 3 of Borgland et al. (2003). In that study, a dopamine neuron was voltage clamped to +40 mV at the soma using a whole cell patch clamp, and the current recorded after stimulation of the slice in the presence and absence of APV was recorded in order to determine the EPSCs due to both NMDA and AMPA receptors and AMPA receptors alone. Figure 6B depicts the model simulation of the same event of glutamate.

We used a square pulse stimulus of glutamate to the kinetic schemes outlined for NMDA and AMPA receptors collocated on the dendritic branches, and the output of the systems was used to drive the gating mechanisms responsible for the affective conductance associated with the NMDA and AMPA currents. As a first approximation, we neglected any time-dependent effects such as plasticity or desensitization. ISIs were calculated using a random number generator with a fixed mean interevent time as outlined in previous studies of background postsynaptic signals. Each ISI in Figure 7 corresponds to the release of glutamate from the presynaptic cleft. Temporal summation of the pulse train generated is largely based on the

duration of the stimulus acting on either NMDA or AMPA receptors, which was deduced from fitting the currents in Fig. 6.

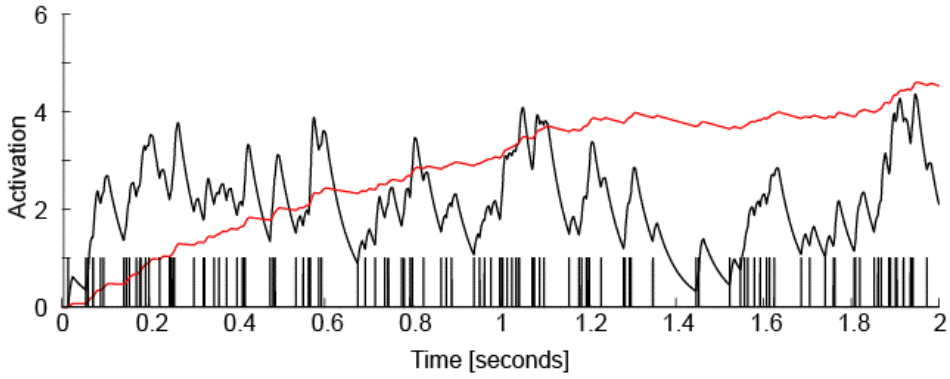

Figure 7: ISI Activity

The effect of summation of hundreds of separate Poisson distributed inputs to the DA neuron demonstrates a relatively tonic activation of both NMDA and AMPA receptor channels. The effect of increasing the mean interevent time increases the frequency of bursts in the simulation. Figure 7 depicts a segment of time in which the pulses of glutamate begin to activate NMDA and AMPA receptors to the point where NMDA begins to gradually rise to a tonic level due to its relatively large time constant.

CVODE, an implicit fifth order Runga-Kutta integration routine with variable step size, was used to obtain the data from the stiff system of differential equations. This procedure brings speed during moments of very predictable behavior of the system using a predictor-corrector method, and the time step is thus increased in magnitude. During portions of the set of differential equations where the integration becomes very complex, the time step is reduced and finer calculations are obtained up to fifth-order accuracy. The CVODE algorithm for integration

thus brings efficiency and accuracy under one unified framework. The simulation was written using Microsoft Visual C++ v6.0 and Matlab v6.0 and run on a Pentium IV 2 GHz processor.

The data were obtained from the simulation after the system of state variables was numerically integrated using CVODE. The 28 state variables were analyzed as a matrix of data entries with columns for each state variable, rows for each time step, utilizing Matlab v6.0. The data was output to various figures for analysis. Limit cycles were observed to evaluate the interactions of certain state variables dynamically. Fourier analysis and individual graphs of certain parameters were also closely plotted to obtain oscillations in the DA model.

Figure 8 shows the average effective total receptor activation for both NMDA and AMPA.

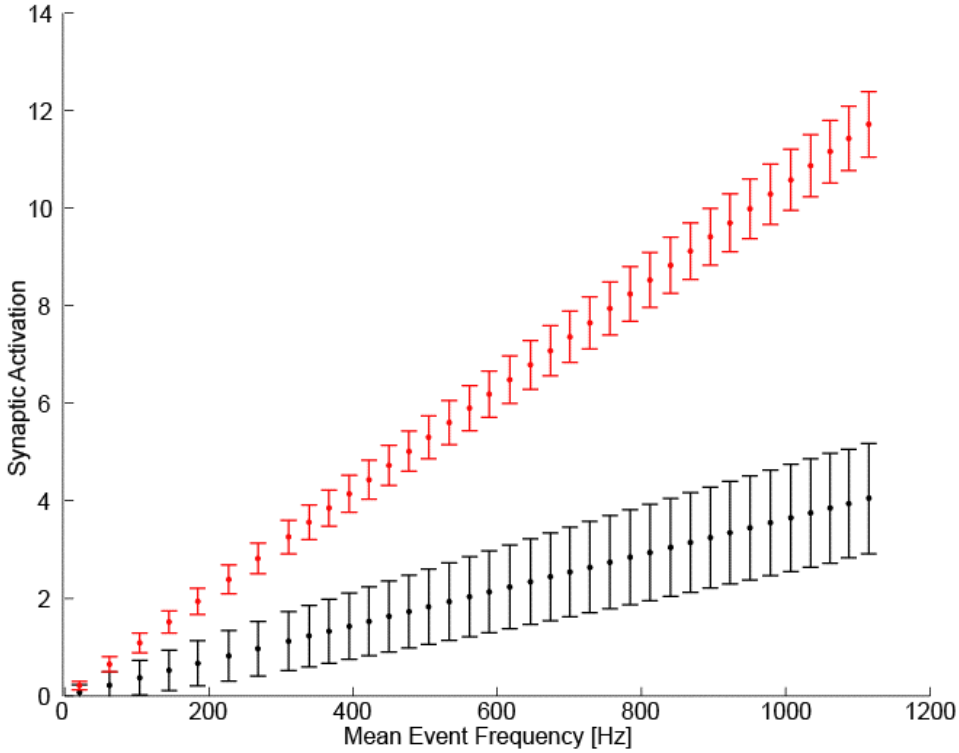

Figure 8: Total Receptor Activation

The variance is larger for AMPA in comparison to NMDA and could account for some of the

variability in the active behavior of the neuron. The receptor activation is also inversely proportional to the mean interevent interval, which can be seen in the analytical argument proposed in Equation 1.15 in the Taylor limit for small <IEI> and β. From these results it can be concluded that for small mean interevent intervals, the average effective conductance for AMPA and average effective permeability for NMDA will vary inversely.

RESULTS

Active behavior such as a spike was counted from the trace of data if the voltage in the soma rose above -30 mV and then below -30 mV over time interval less than 1.5 ms. The time between individual spikes, known as inter-spike intervals (ISI) are used as the criteria for bursting behavior. If there is an ISI of greater than 160 ms which is followed immediately by a first ISI of 80 ms and a second ISI of less than 160 ms, this pattern is considered a burst. These criteria were established both in part due to the literature of prototypical behavior in actual DA neurons in the VTA, and as determined through experiment. Doublets, or two spike "bursts," which occur frequently in the model, were not considered as bursts and have been marked separately.

Figure 9 addresses the issue of granularity implicit in calibration of the model to a single glutamatergic pulse as in Borgland et al. (2003):

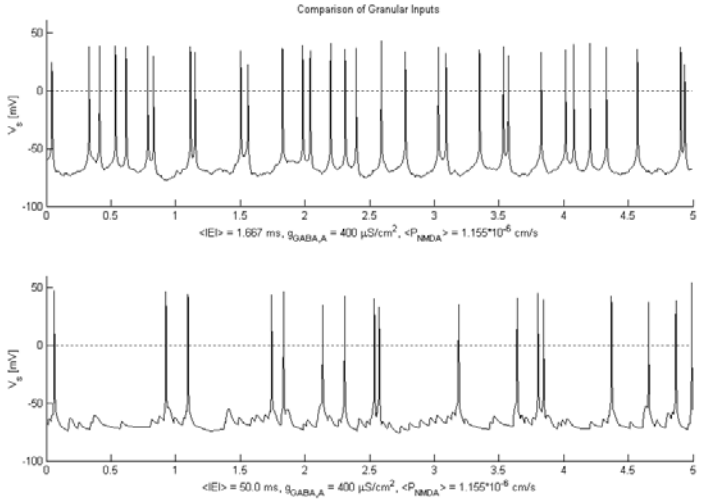

Figure 9: Granularity of Inputs

As this study does not indicate as to the intensity and hence size of receptor recruitment in the

experiment, our simulation of the experimental data assumed a single large activated receptor to produce the results. As such, the scale of multiple inputs to simulations of a number of events occurring over a short period of time was too large and caused unwarranted variability in the voltage traces as can be seen in Figure 9B. To resolve this problem, the mean interevent intervals were reduced using the scaling law of Fig. 8 to produce an effective total receptor behavior which was then scaled by 1/10 before being incorporated into the currents responsible for NMDA and AMPA activity in the model. Figure 9A shows the result of this lowered variability. All experiments were thus performed in this range of lowered mean interevent intervals.

DISCUSSION

Figure 10 shows examples of voltage traces at different values of average P_{NMDA} and $G_{GABA,A}$ inhibition.

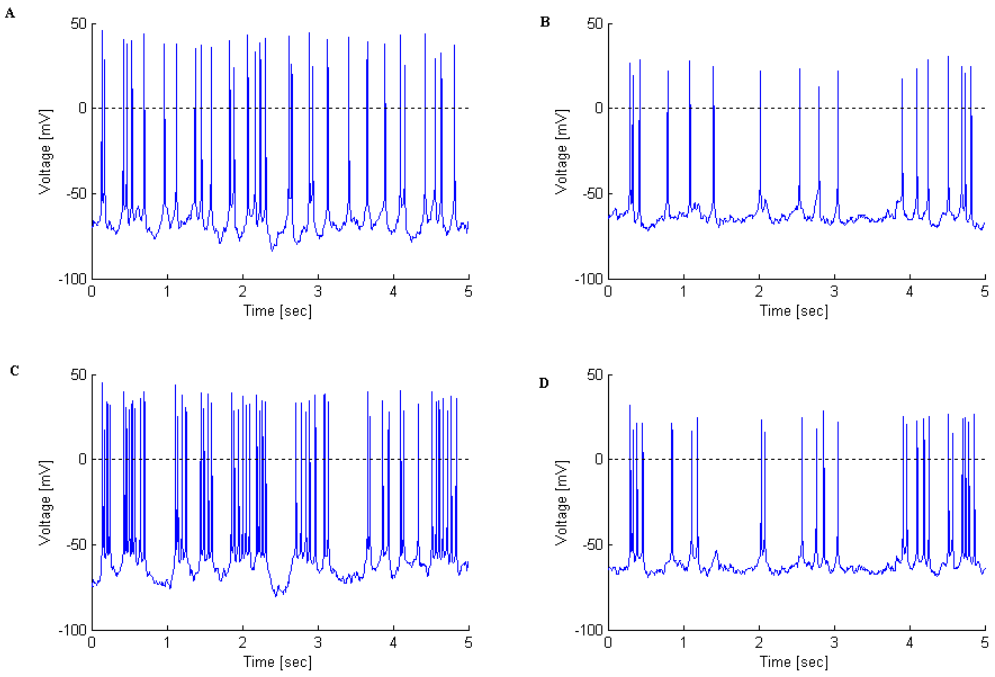

Figure 10: Example of SK Vs. No SK

Figures 10A and 10B are the behavior of the soma in absence of SK blockers and Figures C and D are the same parameter conditions in the presence of SK blockers. Note that traces in absence of SK blockers spike somewhat more regularly, whereas traces in presence of SK blockers spike in bursts. Thus adding the SK current changes the firing pattern from burst firing to single spike firing, just as the work of Seutin et al. (2002), where they observed transitions to bursting in the presence of SK blockers and transitions to single spike firing in the presence of SK agonists *in vivo*. Note also that the average frequency of A and B are 6.2 Hz and 3.4 Hz, respectively, whereas the frequency of B and D are 10.6 Hz and 4.8 Hz, respectively. Not only is frequency

increased for conditions in absence of the SK channel, but GABA,A inhibition tends to decrease the difference between the frequencies of DA neuron pairs with and without SK given identical parameters. Figure 11 shows this difference with more clarity for selected values of GABA,A:

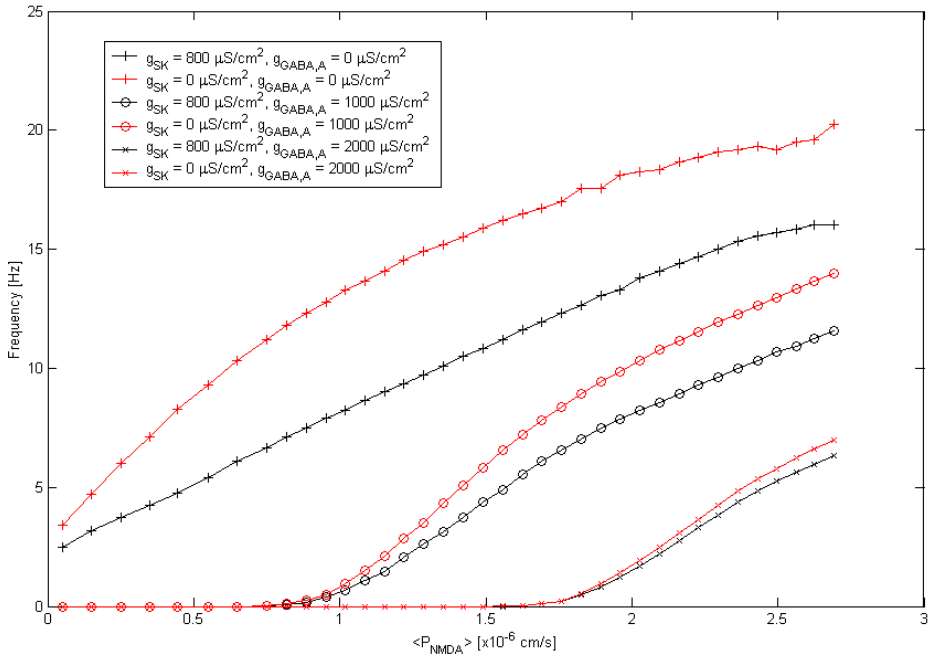

Figure 11: Examples of SK Vs. No SK at Selected GABA,A Levels

Given that the average effective P_{NMDA} varies almost linearly with the mean interevent interval, a grid of mean IEIs and hence effective P_{NMDA} values were selected at regular intervals along with corresponding levels of GABA,A inhibition. Figure 12A and B show the frequency behavior of the neuron in the presence and absence of SK, respectively, with varying levels of P_{NMDA} and tonic $g_{GABA,A}$ inhibition. Note that B reaches regions of higher frequency than A.

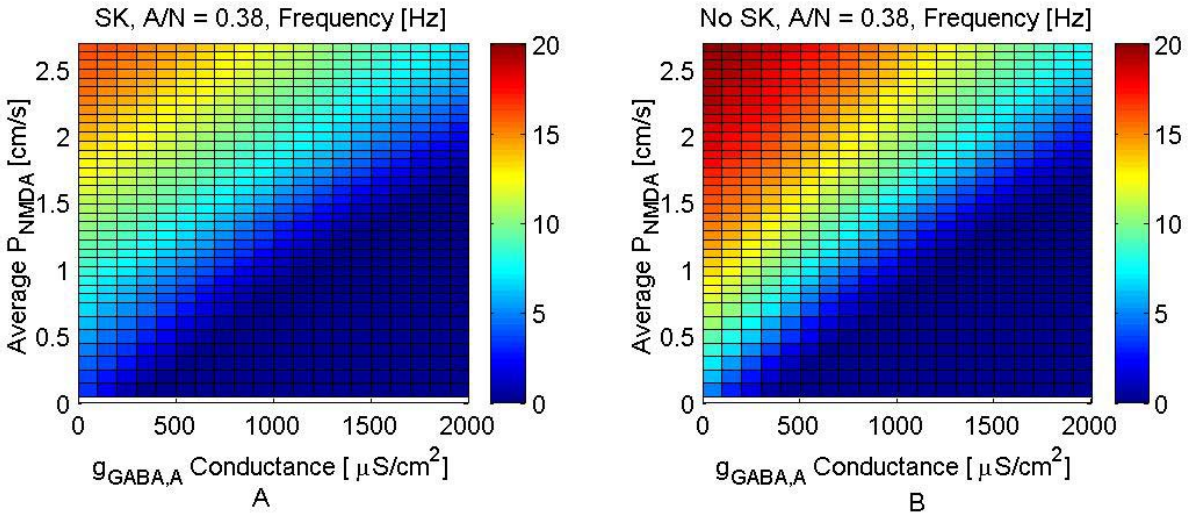

Figure 12: Frequency Plots For A) SK B) No SK

Figure 13 A-D shows examples of varying the ratio of peak AMPA EPSC to NMDA EPSC from the experimentally observed 0.38 to 0.75:

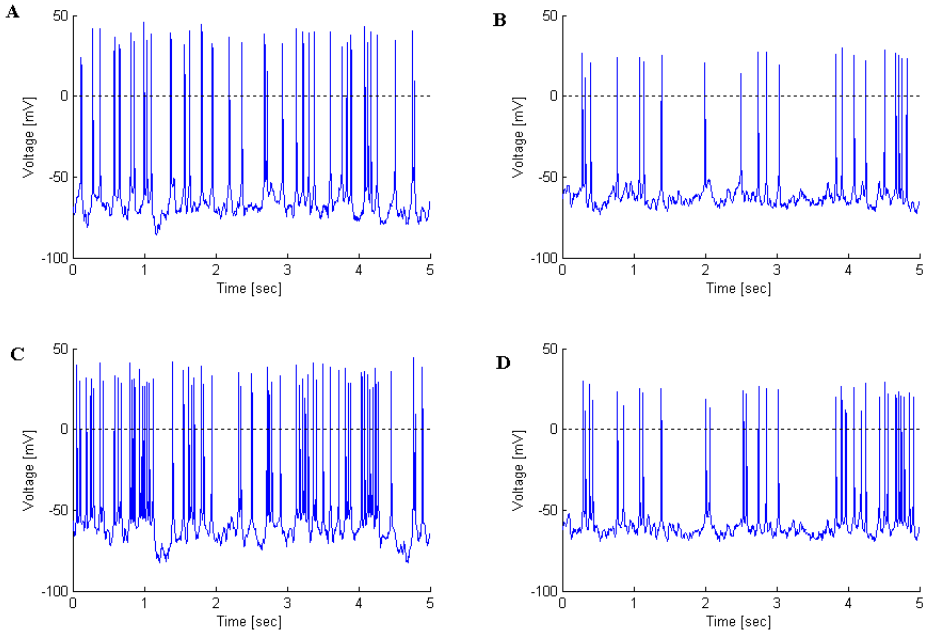

Figure 13: Examples of Traces With Increased AMPA/NMDA (A/N = 0.75)

The increased ratio has been shown experimentally to increase the frequency of the neuron as well as the CV. Our model shows that for a wide range of values, the frequency of the neuron is increased. There is no observed effect on the pattern. Figure 14 A and B show both SK and no SK conditions of the neuron with parameter sweeps identical to that of Figure 12 but with the increased ratio:

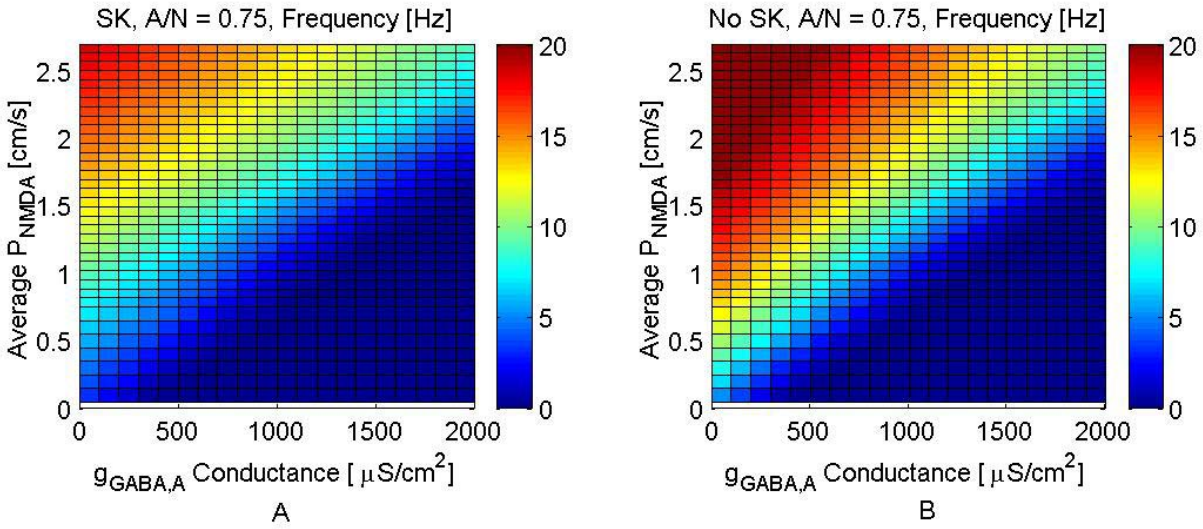

Figure 14: Frequency Plots For A/N = 0.75, A) SK and B) No SK

Note that the high frequency band is much larger with the altered peak AMPA/NMDA ratio.

Figure 15 A-C summarizes the behavior of the DA neuron regarding pattern for effective P_{NMDA} ranging from 0 to $2.7*10^{-6}$ cm/s and gGABA,A from 0 to 2000 μS/cm^2.

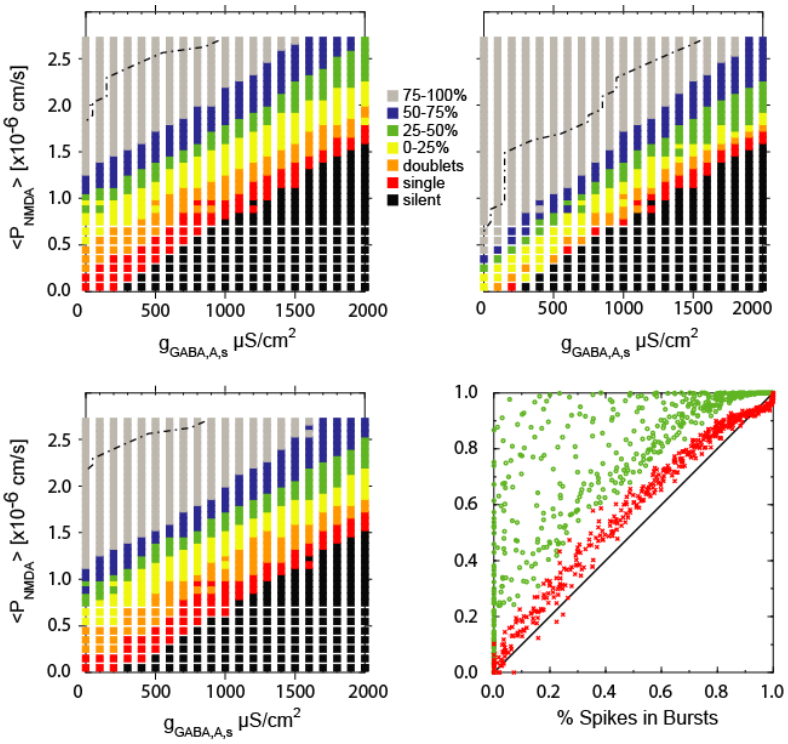

Figure 15: Summary of Pattern for A) SK, B) No SK, C) A/N = 0.75, D) % Spikes in Bursts

Black squares indicate silence, red squares single spike firing (0% spikes fired in bursts and nonzero frequency), yellow < 25% spikes fired in bursts, green < 50% spikes in bursts, blue < 75%, grey >75%, and above dotted line correspond to plateau potentials. The most notable feature is the shrinking of the single spike region present in transition from the neuron possessing SK to the absence of SK. Figure 15D shows that percentage spikes fired in bursts is greatly increased when SK is blocked (green) whereas there is a small difference when increasing the A/N ratio (red).

Figure 16 depicts a scatter plot of simulations of DA neurons where the percentage of spikes fired in bursts is mapped against frequency.

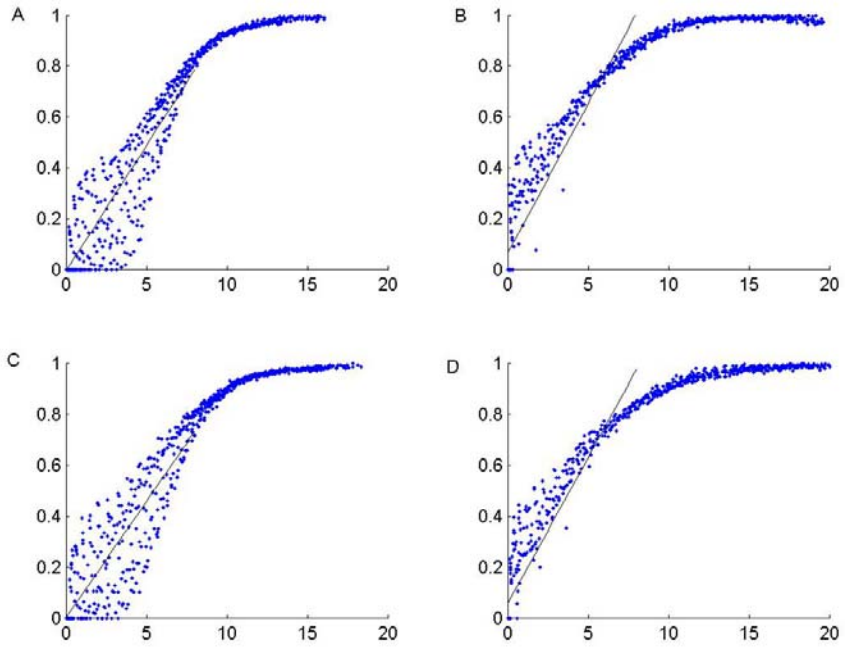

Figure 16: Scatter Plots of Percentage of Spikes in Bursts Vs. Frequency [Hz] For A) SK B) No SK, C) A/N = 0.75, SK, D) A/N = 0.75, No SK

Note that for the cases with SK, the linear correlation of the data is lower as compared to the neuron without SK. Hence as hypothesized, SK tends to cause the neuron to fire in more of a single spike mode as opposed to conditions without this current, where bursting is much more present. Increasing the AMPA/NMDA ratio has little effect on pattern.

CONCLUSION

Random firing of glutamatergic inputs causes substantially more temporal summation at NMDA receptors compared to AMPA regardless of whether the inputs are coherent due to the longer time course of the NMDA inputs. This leads to burst firing at a higher frequency than is observed with tonic activation. The model gives us a glimpse into the stochastic nature of background input to the dopaminergic neuron in an intact human brain.

The firing pattern is dependent on levels of ionotropic glutamatergic and gabaergic input as well as metabotropic inputs that affect the calcium dependent activation of the SK channel. Attentional and motivational states as well as inputs temporally correlated with the presentation of conditioned and unconditioned stimuli related to reward influence the production of bursts *in vivo* and may map onto these three inputs or subpopulations thereof. The time required to evoke a burst is on the order of tens to hundreds of milliseconds, with SK channel blockage being the slowest.

Nonetheless, they provide new and useful information about some of the most basic properties of excitatory synaptic transmission in the VTA. They also provide information that will facilitate the development of pharmacological agents that can be used to probe the role of the VTA in various forms of reinforcement-dependent behavior and perhaps to prevent or alleviate the neural changes that contribute to the development of pathological states such as drug addiction.

The model shows that removing the SK current results in more spikes found in bursts, while increasing GABA,A inhibition tends to decrease the frequency difference between neurons with and without SK. Secondly, increasing the peak EPSC of AMPA with respect to NMDA during an event causes an overall effect of higher frequency observed in the model with little

change in pattern. It has been shown that drug mediated plasticity from a single dose of amphetamine tends to raise the AMPA EPSC with respect to the NMDA EPSC from 0.38 to 0.75, and our model shows that such a change increases the spike frequency with little change in pattern. In fact, modulation of the pattern demonstrates little correlative relationship with firing rate, indicating that the two characteristics are entirely separate phenomena. Finally, the interesting region of parameter space tends to fall along a diagonal band where inhibition and excitation are balanced. This provides for a scope of the activity in a neuron which is far-reaching, including many variations of single spiking and bursting modes.

REFERENCES

Bernheimer H, Birkmayer W, Hornykiewicz, Jellinger K, and Seitelberger F. Brain dopamine and the syndromes of Parkinson and Huntingdon. Clinical, morphological, and neurochemical correlations. J. Neurosci., 20:415–455, 1973.

Bonci A and Malenka RC. Properties and plasticity of excitatory synapses on dopaminergic and GABAergic cells in the ventral tegmental area. J. Neurosci. 19:3723-3730, 1999.

Borgland SL, Malenka RC, and Bonci A. Acute and chronic cocaine-induced potentiation of synaptic strength in the ventral tegmental area: electrophysiological and behavioral correlates in individual rats. J. Neurosci., 24:7482–7490, 2004.

Brodie MS, McElvain MA, Bunney EB, and Appel SB. Pharmacological reduction of small conductance calcium activated potassium current (SK) potentiates the excitatory effect of ethanol on ventral tegmental area dopamine neurons. J. Phamacol. Exp. Ther., 290:325–333, 1999.

Canavier CC. Sodium dynamics underlying burst firing and putative mechanisms for the regulation of the firing pattern in midbrain dopamine neurons: A computational approach. Journal of Computational Neuroscience, 6:49–69, 1999.

Charlety PJ, Grenhoff J, Chergui K, Svensson TH, and Chouvet G. Burst firing of mesencephalic dopamine neurons is inhibited by somatodendritic application of kynurenate. Acta Physiologica Scandinavica, 142:105–112, 1991.

Chergui K, Charlety PJ, Akaoka H, Saunier CF, Brunet J-L, Buda M, Svensson TH, and Chouvet G. Tonic activation of NMDA receptors causes spontaneous 26 burst discharge of rat midbrain neurons in vivo. Eur. J. Neurosci., 5:137–144, 1993.

Chergui K, Nomikos GG, Methe JM, Gonon FG, and Svensson TH. Burst stimulation of the medial forebrain bundle selectively increases fos-like immunoreactivity in the limbic forebrain of the rat. Neuroscience, 72:141–156, 1996.

Destexhe A., Mainen ZF, and Sejnowski TJ. Fast kinetic models for simulating AMPA, NMDA, GABAA and GABAB receptors. In: The Neurobiology of Computation, edited by Bower, J., Norwell, MA; Kluwer Academic Press, pp. 9-14, 1995.

Fa M, Mereu G, Ghiglieri V, Meloni A, Salis P, and Gessa GL. Electrophysiological and pharmacological characteristics of nigral dopaminergic neurons in the conscious, head-restrained rat. Synapse, 48:1–9, 2003.

Fiorillo CD and Williams JT. Glutamate mediates an inhibitory postsynaptic potential in dopamine neurons. Nature, 394:19–21, 1998.

Freeman AS, Meltzer LT, and Bunney BS. Firing properties of substantia nigra dopaminergic neurons in freely moving rats. Life Sciences, 36:1983–1994, 1985.

Grace AA and Bunney BS. The control of firing pattern in nigral dopamine neurons: Single spike firing. J. Neurosci., 4:2866–2876, 1984a.

Grace AA and Bunney BS. The control of firing pattern in nigral dopamine neurons: Burst firing. J. Neurosci., 4:2877–2890, 1984b.

Hyland BI, Reynolds JNJ, Hay J, Perk CG, and Miller R. Firing modes of midbrain dopamine cells in the freely moving rat. Neuroscience, 1 14:475–492, 2002.

Johnson SW, Seutin V, and North RA. Burst-firing in dopamine neurons induced by N-methyl-D-aspartate: Role of electrogenic sodium pump. Science, 258:665–667, 1992.

Johnson SW and Wu Y-N. Multiple mechanisms underlie burst firing in rat midbrain dopamine neurons in vitro. Brain Res., 1019:293–296, 2004.

Jones S and Bonci A. Synaptic plasticity and drug addiction. Current Opinion in Pharmacology, 5:20–25, 2005.

Komendantov AO, Komendantova OG, Johnson SW, and Canavier, CC. A modeling study suggests complimentary roles for GABAA and NMDA receptors and the SK channel in regulating the firing pattern in midbrain dopamine neurons. J. Neurophysiol. 91: 346-357, 2004.

Margolis EB, Hjelmstad GO, Bonci A, and Fields HL. Both kappa and mu opioid agonists inhibit glutamatergic input to ventral tegmental area neurons. J. Neurophysiol., 93:3086–3093, 2005.

Mereu G, Lilliu V, Casula A, Vargiu PF, Diana M, Musa A, and Gessa GL. Spontaneous bursting activity of dopaminergic neurons in midbrain slices from immature rats: Role of N-methyl-D-aspartate receptors. Neuroscience, 77:1029–1036, 1997.

Overton P and Clark D. Iontophoretically administered drugs acting at the N-methyl-Daspartate receptor to modulate burst firing in A9 dopamine neurons in the rat. Synapse, 10:131–140, 1992.

Paladini CA and Tepper JM. GABAA and GABAB antagonists differentially affect the firing pattern of substantia nigra dopaminergic neurons in vivo by decreasing input resistance. Synapse, 32:165–176, 1999.

Paladini CA, Fiorillo CD, Morikawa H, and Williams JT. Amphetamine selectively blocks inhibitory glutamate transmission in dopamine neurons. Nat. Neurosci., 4:275–281, 2001.

Ping HX and Shepard PD. Apamin-sensitive Ca2+-activated K+ channels regulate pacemaker activity in nigral dopamine neurons. NeuroReport, 7:809–814, 1996.

Schultz W. Predictive reward signal of dopamine neurons. J. Neurophysiol., 80:1–27, 1998.

Seutin V, Johnson SW, and North RA. Apamin increases NMDA-induced burst firing of rat mesencephalic dopamine neurons. Brain Res. 630:341-4.

Ungless MA, Whistler JL, Malenka RC and Bonci A. Single cocaine exposure in vivo induces long-term potentiation in dopamine neurons. Nature 411: 583-586, 2001.

Wang T, French ED. Electrophysiological evidence for the existence of NMDA and non-NMDA receptors on rat ventral tegmental dopamine neurons. Synapse 13:270 –277. 1993.

Wang T, French ED. NMDA, kainate, and AMPA depolarize nondopamine neurons in the rat ventral tegmentum. Brain Res Bull 36:39–43. 1995.

Wang T, O'Connor WT, Ungerstedt, U and French ED. N-Methyl-D-aspartic acid biphasically regulates the biochemical and electrophysiological response of A10 dopamine neurons in the ventral tegmental area: in vivo microdialysis and in vitro electrophysiological studies. Brain Research 666: 255-262, 1994.

Weinberger DR. Implications of normal brain development for the pathogenesis of schizophrenia. Arch. Gen. Psychiatry, 44:660–669, 1987.

Wolfart J, Neuhoff H, Franz O, and Roeper J. Differential expression of the smallconductance, calcium activated potassium channel SK3 is critical for pacemaker control in dopaminergic midbrain neurons. J. Neurosci., 21:3443–3456, 2001.

Wu Y-N and Johnson SW. Pharmacological characterization of inward current evoked by N-methyl-D-aspartate in dopamine neurons in the rat brain slice. J. Pharmacol. Exp. Ther., 279:1–7, 1996.

Zhang HF, Hu HT, White FJ, and Wolf ME. Increased responsiveness of ventral tegmental area dopamine neurons to glutamate after repeated administration of cocaine or amphetamine is transient and selectively involves AMPA receptors. J. Pharmacol. Exp. Ther., 281:699–706, 1997.

Zhang J, Chiodo LA, and Freeman AS. Influence of excitatory amino acid receptor subtypes on the electrophysiological activity of dopaminergic and nondopaminergic neurons in rat substantia nigra. J. Pharmacol. Exp. Ther., 269:313–321, 1994.

Zigmond MJ, Abercrombie ED, Berger TW, Grace AA and Stricker EM. Compensations after lesions of central dopaminergic neurons: some clinical and basic implications. Trends Neurosci., 13:290-296.

VITA

The author, Richard S. Landry, Jr., was born in New Iberia, Louisiana where he lived with his parents Richard and Mary, his brother William, and his dog, Bacchus. He attended Tulane University from 1997 to 2001 where he majored in biomedical engineering, physics, and math. After graduation he began his work as a computational neuroscientist while attending graduate school at the University of New Orleans for a Masters Degree in Applied Physics. He has worked as a teaching assistant for linear algebra and general physics labs, a computer technician, a researcher in quantum coherent control experiments, and as a computational neuroscientist. Due to the deluge of hurricane Katrina, he moved to Chicago with his girlfriend Marlo to find employment and further his graduate education.